Pergamon
www.elsevier.com/locate/asr

Adv. Space Res. Vol. 29, No. 6, pp. 815–823, 2002

Printed in Great Britain
0273-1177/02 $22.00 + 0.00
PII: S0273-1177(02)00037-6

RECENT ADVANCES IN TOPSIDE PROFILE MODELING

S. A. Pulinets[1], V. H. Depuev[1], A.T.Karpachev[1], S. M. Radicella[2], and N. P. Danilkin[3]

[1] *Institute of Terrestrial Magnetism, Ionosphere and Radiowave Propagation, Russian Academy of Sciences, (IZMIRAN), Troitsk, Moscow Region, 142190, RUSSIA*
[2] *Abdus Salam International Centre for Theoretical Physics, Strada Costiera 11, 34014 Trieste, ITALY*
[3] *Institute of Applied Geophysics, Rostokinskaya, 9, Moscow, 129226, RUSSIA*

ABSTRACT

A parameterized model for topside profile was developed based on the Epstein function approximation. Using the Intercosmos-19 database, model parameters were obtained for different geophysical conditions, including strong magnetic storms. In some specific conditions the F3 layer was observed on topside ionograms. A physical explanation is proposed as well as results based on modeling approach. Topside ionograms from the sounder on MIR Space Station were studied. Some exotic cases are presented including oblique propagation, station position under the peak height etc. Peak height global distribution is described as well as neutral wind parameters derived from the topside peak height values. © 2002 COSPAR. Published by Elsevier Science Ltd. All rights reserved.

INTRODUCTION

One of the reasons for poor representation of the topside vertical profiles by empirical models is the very small database of topside profiles. For example, International Reference Ionosphere model uses the Alouette and ISIS satellites database obtained mainly for American sector of longitudes. The strong longitudinal effect in the ionosphere (Ben'kova et al., 1990) leads to essential discrepancy of the experimental data and IRI for other longitudinal sectors. It is shown in Figure 1 (Karpachev et al., 1993). We selected for comparison the data of topside sounding at 60° DIP latitude for both hemispheres: for summer solstice nighttime conditions (in Northern hemisphere) and high solar activity period. At the left panel, the IRI-90 and satellite peak density global longitudinal distributions are shown. One can see the maximal discrepancy at ~300° E in the Northern hemisphere, and ~200° E in the Southern one. From the right panel where the individual topside profiles comparison with IRI in extreme discrepancy points for both hemispheres is shown, we realize that the problems exist not only in the peak

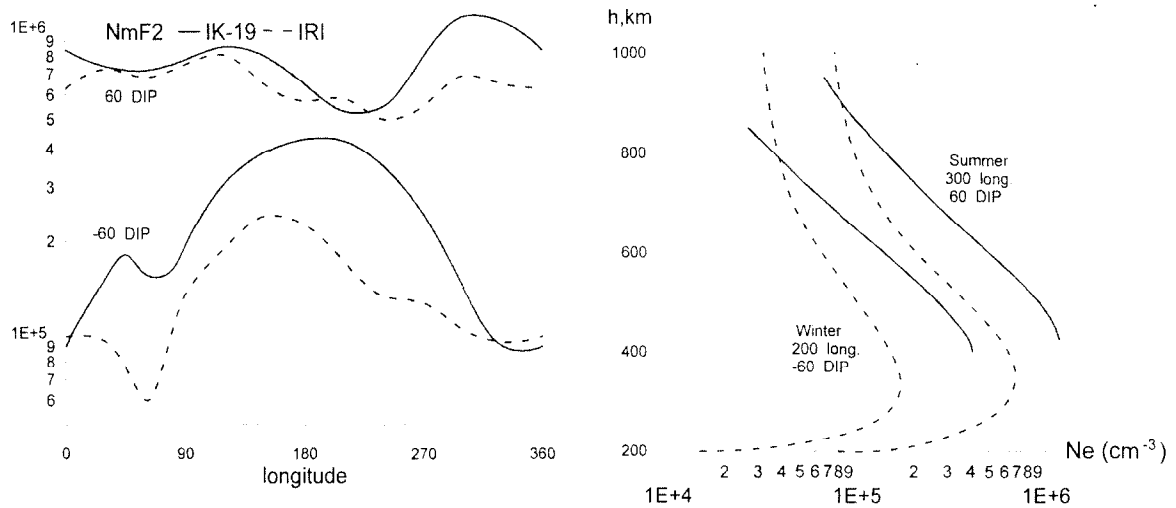

Fig.1 Comparison of empirical data scaled from Intercosmos-19 topside sounding ionograms (solid lines) and IRI-90 model (dashed lines). Longitudinal distribution of NmF2 for ± 60° DIP latitude (summer solar solstice nighttime conditions) – left panel. Vertical topside profiles (solid lines) and IRI-90 profiles (dashed lines) for selected longitudes at ± 60° DIP latitude – right panel

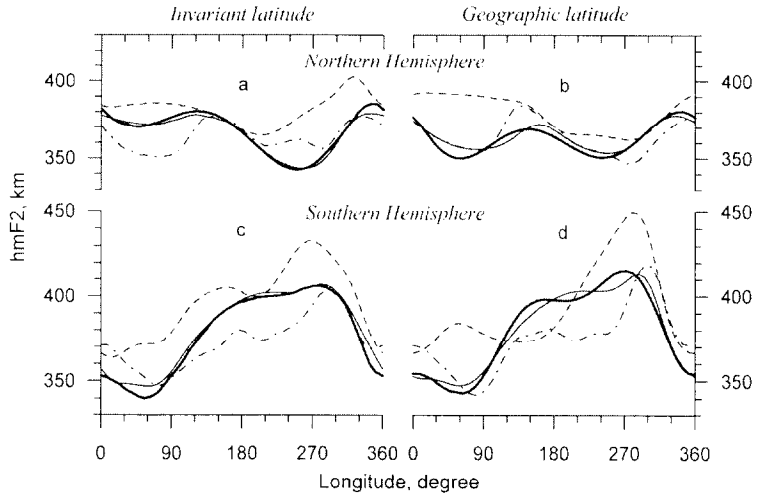

Fig.2. Longitudinal variations of *hmF2* obtained from Intercosmos-19 data (thick lines) and IRI-90 model (dash-dotted lines) and calculated from neutral wind derived by means of regularization method (thin lines) and from HWM model (Hedin et al., 1991) (dashed lines) for the night-time (22 LT) summer conditions at ±40° of invariant (a, c) and geographic (b, d) latitudes in the Northern hemisphere (a, b) and in the Southern one (c, d).

density values but also with the whole profile description including the scale height, peak altitude, transition point etc. These results are supported by more recent studies of global distribution of hmF2 connected with the deviation of neutral wind parameters (Karpachev and Gasilov, 2000). The experimentally derived hmF2 longitudinal distributions compared with the IRI and HWM model (Hedin et al., 1991) models are shown in Figure 2. Again we see essential discrepancies for different longitudinal sectors in both hemispheres observed as along DIP and geographical latitudes. These evident motivated our forced activity in data processing of Intercosmos-19 and Cosmos 1809 satellites (Pulinets, 1989). The topside profile database of Pulinets (1999) (http://antares.izmiran.rssi.ru/projects/IK19/) was used for elaboration of parameterized empirical model of the topside profiles of electron concentration.

PARAMETERISED EMPIRICAL MODEL OF TOPSIDE VERTICAL PROFILES

Radicella and Chang (1995) showed that the topside profile could be approximated by Epstein function:

$$N(z)=4.0*\frac{N_0\exp\left(\frac{z}{B2u}\right)}{\left(1+\exp\left(\frac{z}{B2u}\right)\right)^2}$$

B2u characterizes the topside layer thickness and changes linearly with the height: $B2_u=B_{i)}+k\times z$, $z = h - h_{max}$. As a first approach approximately 4000 topside profiles were used for daytime (11-16 LT) and nighttime (22-04 LT) conditions to parameterize the topside profiles within the range ± 80° DIP. To avoid the paper overloading by tables, the results of parameterization are shown in Figure 3. We divided the database into three groups by season: winter, equinox and summer. Each group is presented by a separate curve. The detailed analysis of the presented model will be the subject of separate paper.

DISTURBED CONDITIONS

The same technique was applied for topside profiles parameterization during geomagnetically disturbed conditions. On the left panel of the Figure 4 the latitudinal cross-sections of the peak parameters (two upper panels) and the *B2u0* coefficient (bottom panel) for three stages of geomagnetic storm are presented. They are compared with the quasitomographic reconstruction of the ionosphere proposed by Nava et al. (2001). The bottom side of the ionosphere is simulated by a NeQuick model (Leitinger et al., 1999) derived profile where the F2 peak values (*NF2m* and *HmF2*) are those of the experimental satellite topside profile. The *foF1* and *foE* values used are obtained from simplified models that take into account time, season and solar activity The ionosphere expansion during main phase of the geomagnetic storm is evident as from the *B2u0* coefficient behavior so from the ionosphere vertical cross-section presented on the right panel of the Figure 4. A similar effect of ionosphere

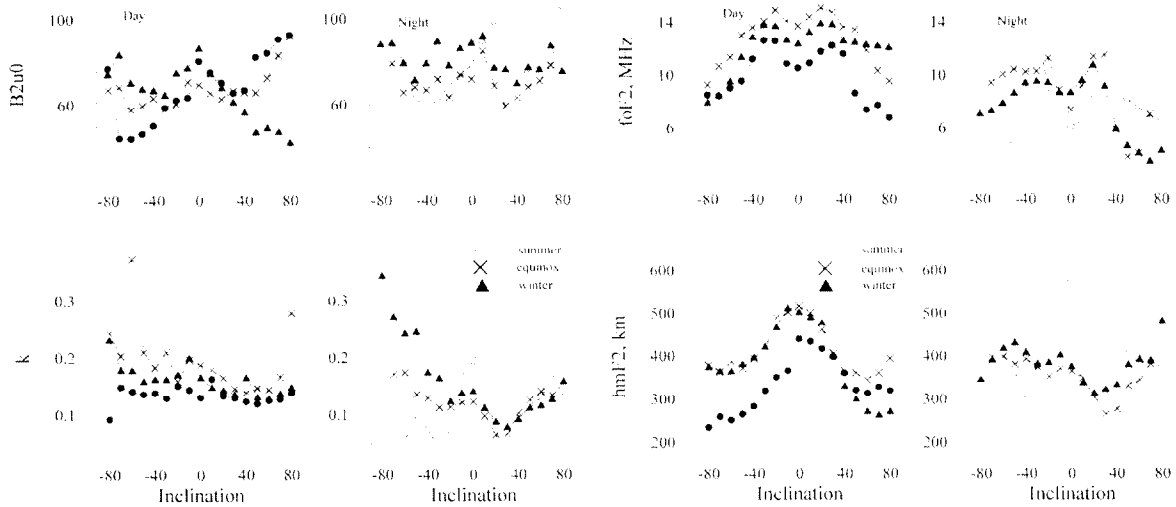

Fig. 3 The parameterized model of topside electron concentration vertical profile from Intercosmos-19 database. The model coefficients presented for three seasons in the left panel, and the peak parameters for the same conditions in the right panel

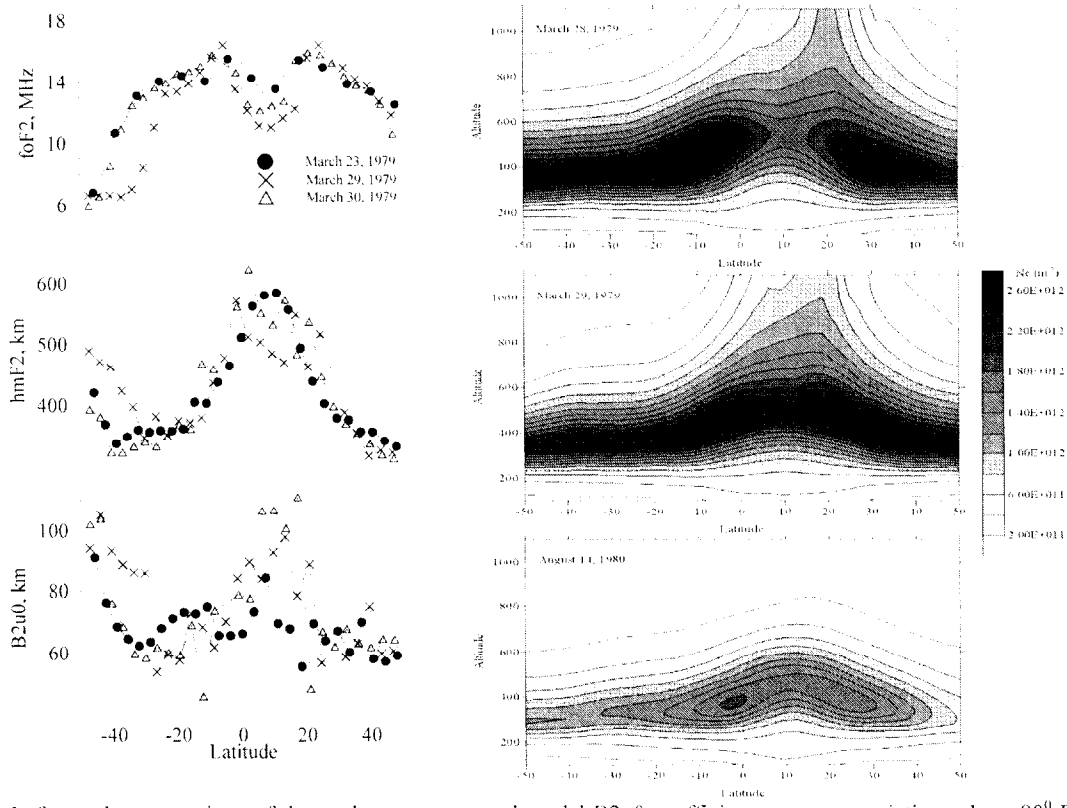

Fig. 4. Left panel - comparison of the peak parameters and model B2u0 coefficient pre-noon variations along 90^0 E longitude during slightly disturbed (March 23, 1979) conditions and different phases of the magnetic storm (March 29-30, 1979). Right panel – quasitomographic reconstruction of the vertical ionosphere cross-section for the same cases.

expansion is observed locally over the regions of seismic activity (Pulinets and Legen'ka, 2001) when the ionosphere is disturbed by the approaching earthquake (Pulinets, 1998) within the time span of 1-5 days before the seismic shock. The only difference between the cases is that in addition to the ionosphere expansion a mean ion mass drop is observed in the seismically disturbed ionosphere which is contrary to geomagnetically disturbed ionosphere where the mean ion mass increases due to changes of the mass relation ([N2] + [O2]) / [O]).

F3 LAYER OBSERVATIONS FROM ONBOARD THE SATELLITE

Depuev and Pulinets (2001, see also reference therein) reported recently on the observation of additional ionization layer from onboard the Intercosmos-19 satellite, the so called F3 layer. They made attempt to estimate the spatial scale of the observed phenomenon in addition to previously published cases of observation and theory. It was demonstrated that the F3 layer is observed within the range ± 10° DIP in daytime equinox conditions (Figure 5,

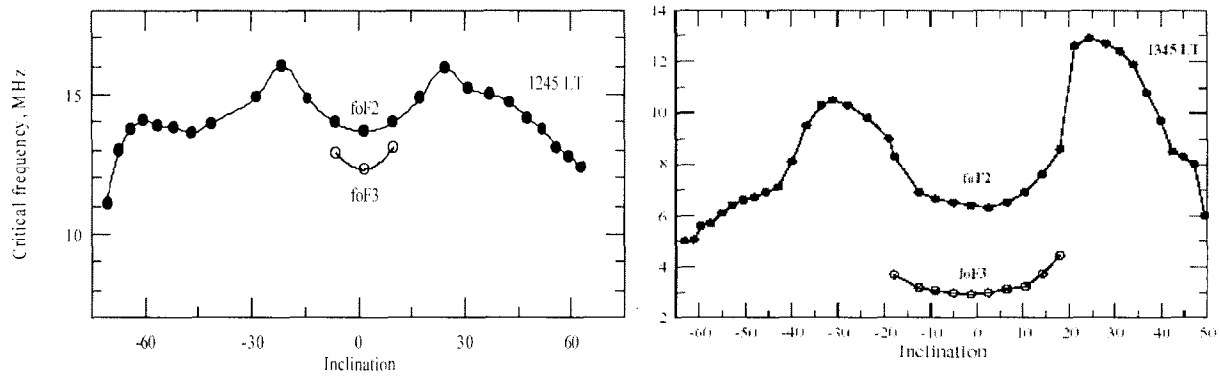

Fig. 5. Critical frequencies scaled from topside ionograms along the satellite pass: foF2 – closed circles, foF3 – open circles. Left panel presents the data for 26 of March 1979 (Intercosmos-19 satellite, right panel – 05 of June 1987 (Cosmos 1809 satellite)

left panel). Nighttime F3 layer observations were reported also. The data published relate to high solar activity period. To create a model of the observed phenomena in addition to theoretical attempts, as much experimental data should be collected as possible for different geophysical conditions. In addition to the equinox conditions reported in previous papers the F3 layer was observed in summer solstice conditions by Cosmos 1809 satellite. Figure 6 demonstrates the sequence of topside ionograms registered during daytime at equatorial ionosphere on June 05, 1987 during extremely quiet geomagnetic conditions (Ap=7). One can clearly see the distinct additional layer manifested as an additional ledge on topside ionograms. Figure 5 presents a comparison of critical frequencies scaled from ionograms for Intercosmos-19 (left) and Cosmos 1809 (right). It shows a more extended (in latitude) F3 layer in the Cosmos 1809 data, practically from crest to crest of the equatorial anomaly (± 19° DIP). The small asymmetry in critical frequencies is the seasonal effect because data are collected during solar solstice. The most pronounced difference is the difference between the F3 and F2 critical frequencies. The difference foF2-foF3 is much larger in the Cosmos 1809 data than in the Intercosmos-19 data, although the magnitude of the overall frequencies for Cosmos 1809 is lower due to low solar activity period. The F3 layer altitude is almost the same: ~750 km at −1.2 DIP.

PLASMA DEPLETIONS AND PLASMA BUBBLES

It was reported earlier on the extremely low densities registered in the topside equatorial (Benson and Brinton, 1983 and references therein) and polar (Brinton et al., 1978) ionosphere. Such plasma cavities were classified as plasma bubbles and polar holes respectively. The plasma bubbles observed by topside sounding technique were reported also in (Dyson and Benson, 1978). In this regard we want to report that similar depletions could be observed also in the main trough region (Muldrew, 1965). We can say that sometimes the ionosphere collapse is observed when the critical frequency approaches right up to the local upper hybrid frequency at the altitude of the satellite which is near 960 km. The topside ionogram is observed as practically vertical trace and it is impossible to calculate the vertical ionization profile. In such cases radio imaging of the ionosphere by means of swiping radiospectrometer (Pulinets, 1990; Rothkaehl et al., 1992) could help. The signals from broadcast transmitters and other ground based HF transmitters start to penetrate into the topside ionosphere at the vicinity of the critical frequency value. Scaling the envelope of the noises from the satellite HF radiospectrometer one can easily estimate the critical frequency value. In case of Cosmos 1809 satellite, the HF signal intensity value was measured just before the sounding at input of the receiver of the IS-338 topside sounder on the satellite. The dynamic spectrum shows the whole structure of the ionosphere along the satellite pass. Such radio image of the ionosphere demonstrates much more details on the ionosphere structure and physical processes within the ionosphere in addition to the density information. One can extract from the images the information on the electron temperature anisotropy, precipitating particle fluxes in auroral regions, cusp position etc. But it is the subject of the separate paper. We will concentrate here only on extremely low density registered on such dynamic spectrum. Figure 7

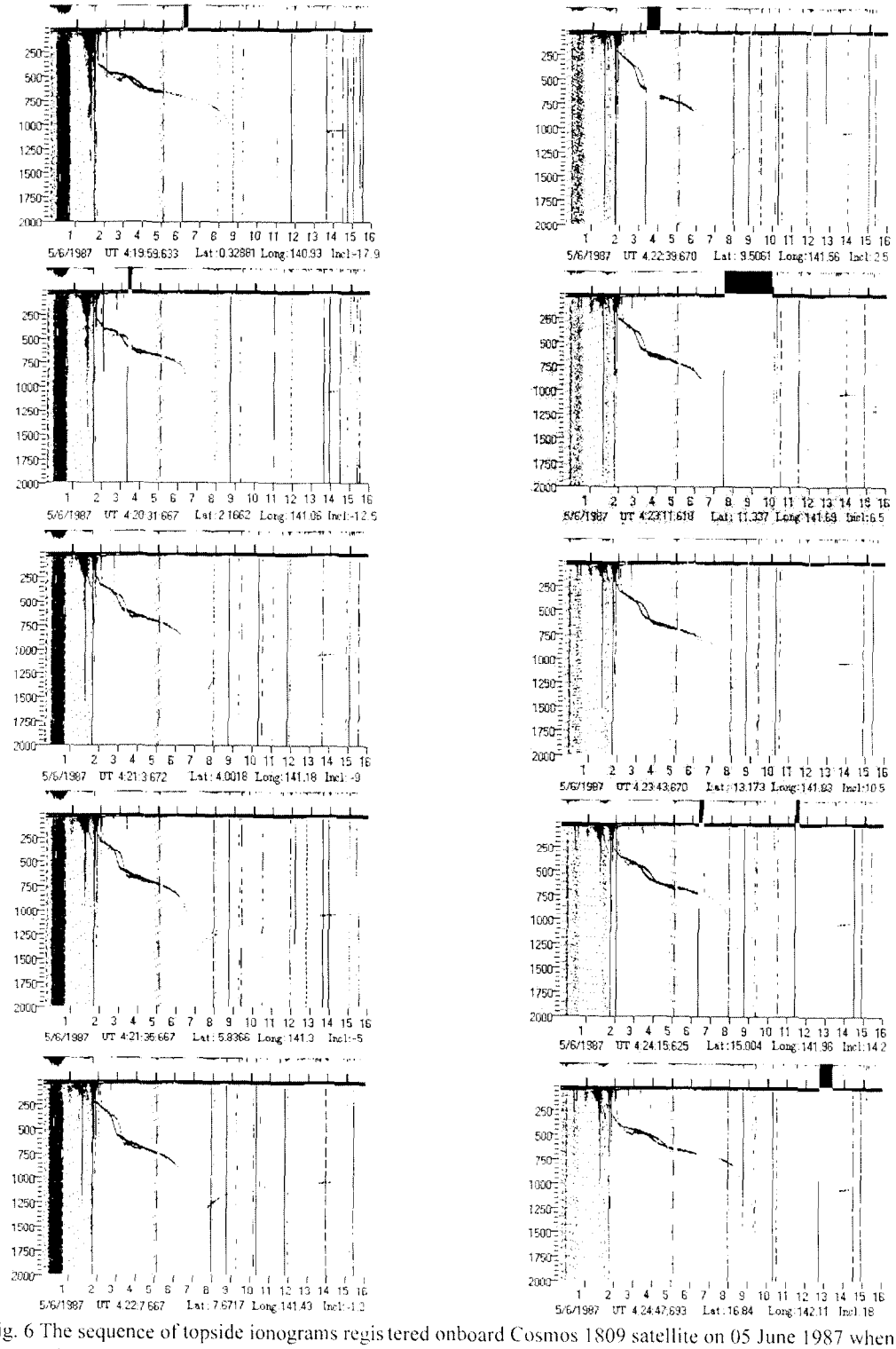

Fig. 6 The sequence of topside ionograms registered onboard Cosmos 1809 satellite on 05 June 1987 when F3 layer was observed in equatorial ionosphere at 140° E longitude

illustrates the dynamic spectrum collected on June 16-17, 1987 (top panel) and the topside ionogram collected at the moment marked by arrow on the dynamic spectrum (bottom panel). As one can see, the critical frequency is of the order of 1.1 MHz corresponding to $NmF2 \sim 1.5 \cdot 10^4$ cm^{-3} and is very close to the local upper hybrid frequency at the satellite height which is nearly 0.8 MHz. The local plasma frequency at the satellite vicinity is of order 10^3 cm^{-3}.

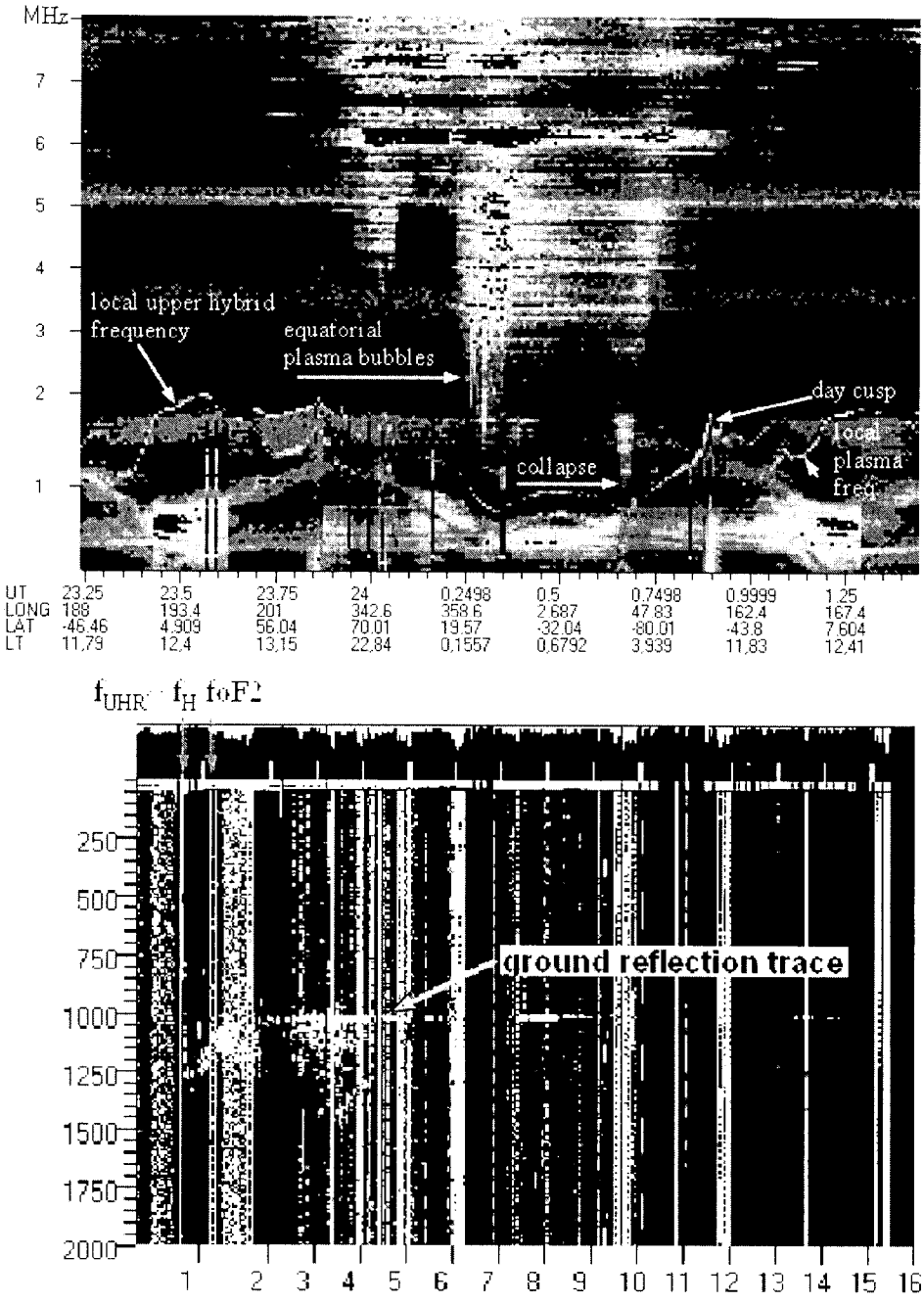

Fig. 7. Radio image of the ionosphere by means of topside sounder receiver input processing within the band 0.3 – 8 MHz on 16-17 of June 1987 (top panel). The topside ionogram corresponding to the case of the ionosphere collapse at the main ionospheric trough in nighttime Southern hemisphere (bottom panel). 01:45 LT, Ilat~57.5°, Lat=-63.7°, Long=11.7°

In the same figure (top panel), at the nighttime equatorial ionosphere, one can see sporadic depletions which we interpret as plasma bubbles. Due to the high altitude of the Cosmos 1809 satellite orbit (960 km) the bubbles do not float up to the satellite height. This situation is contrary to the case of the Intercosmos-19 satellite when sometimes it is to be found inside a plasma bubble. In this case we obtain very interesting ionograms, which are shown in Figure 8. To not overload the paper we do not present the whole sequence of the ionograms but only those just before entering the bubble (Fig.8 a), on the input border of the bubble (Fig 8 b), inside the bubble (Fig. 8 c), at the output border of the bubble (Fig. 8 d), and just outside the bubble (Fig. 8 e). The satellite moved from

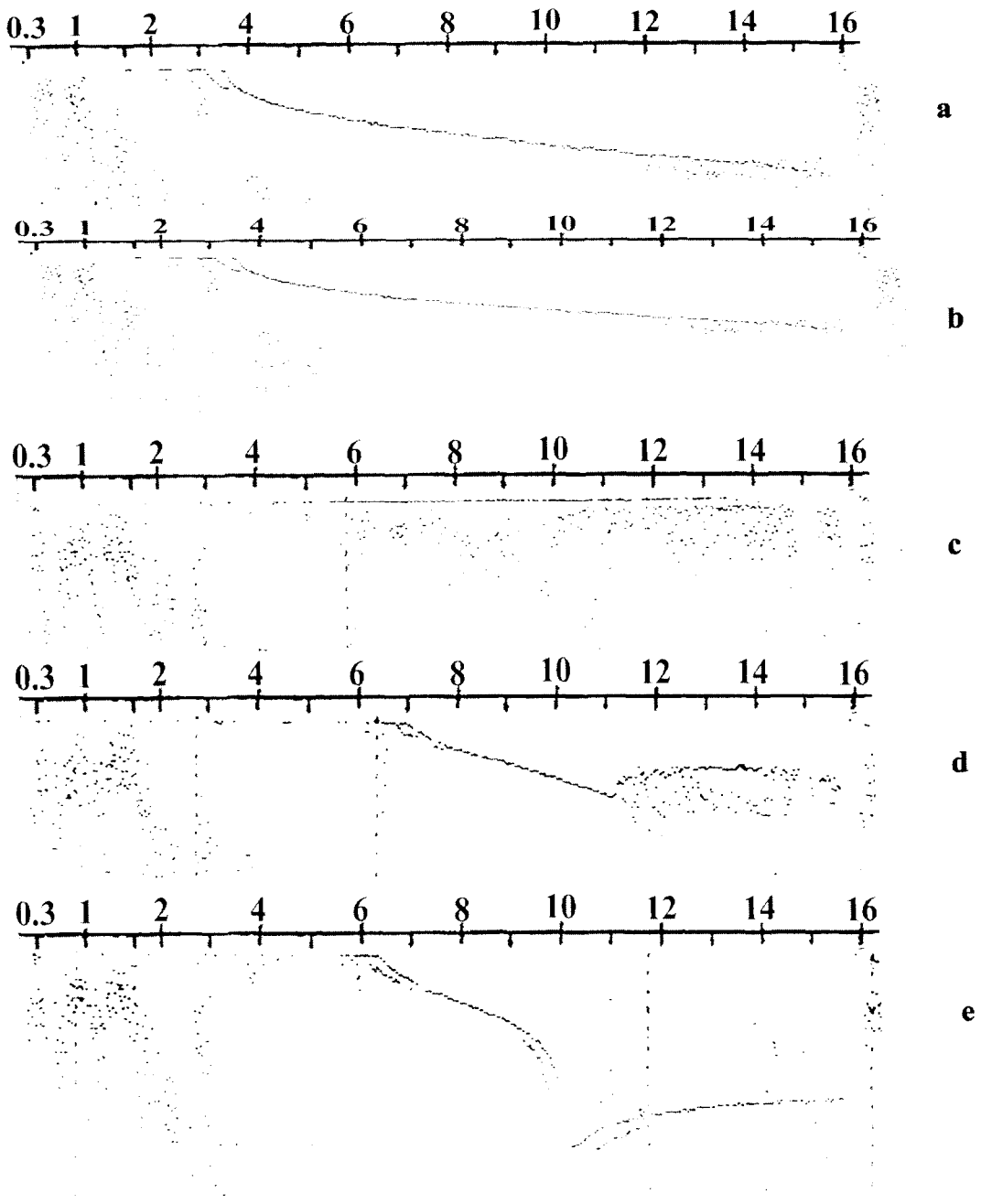

Fig. 8. The sequence of Intercosmos-19 topside ionograms when satellite was passing through plasma bubble. "a" – φ=20.7°, "b" – φ=17°, "c" – φ=-13.1°, "d" - φ=-20.8°, "e" - φ=-24.6°

North to South in a longitudinal band 125°-135° E in the nighttime equatorial ionosphere (21 MLT) during winter solstice (December 20, 1979), high solar activity period. During this part of trajectory, the satellite height changed from 779 km (Fig. 8 a) to 604 km (Fig. 8 e) . In Figure 8 c we see the horizontal line within the frequency band 5.5 MHz – 13.5 MHz. It is interpreted as a bubble with very dense walls so the signal cannot propagate outside the bubble cavity. Similar cases were observed onboard the MIR Space Station with a much lower orbital altitude (nearly 360 km) (Danilkin, 2000). The presented sequence could be interpreted also as bottomside traversal under the peak height of the F-layer. In this case, however, based on results from soundings on the orbital MIR Space Station which is regularly immersed into the bottomside ionosphere, ionogram "c" is interpreted as a topside ionogram because such reflection are not observed in the bottomside.

MIR SPACE STATION RADIO SOUNDING EXPERIMENTS

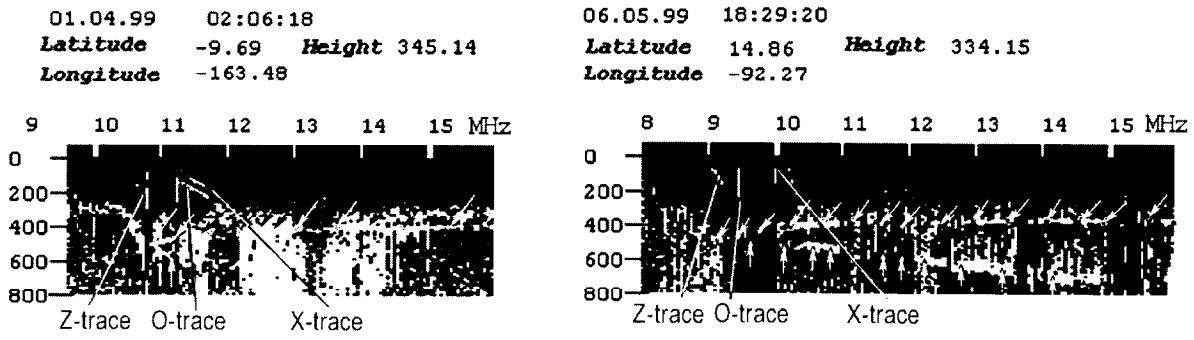

Fig. 9. Fragments of ionograms obtained from the MIR Space Station while it was under the F-2 layer peak.

A replica of IS-338 topside sounder was installed onboard the orbital MIR Space Station. This experiment was conducted to check the possibility of the ionosphere monitoring using topside sounder on a low orbiting satellite (Danilkin, 2000). The experiment clearly demonstrated that even for cases of sounding under the peak the critical frequency could be determined and globally monitored as illustrated in Figure 9. Both panels correspond to cases when the station was under the F2 peak. Note that the ground reflection designated on the figure by slanting arrows finishes at frequencies lower than the local cut-off frequencies. For topside sounding the ground reflection trace and topside reflection trace should merge at the critical frequency. It means that the traces on the ionogram (left panel) designated as O-trace and X-trace are reflections from the above the satellite, because the peak of F2 layer is over the station. But the ground reflection finishes at the local plasma frequency, which is lower than the critical frequency. The most intriguing is the trace marked by vertical arrows and situated lower than the ground reflection trace. It is a ray, which was reflected from the ground, then reflected from the peak height and returned to the satellite. That's why the delay is the sum of ground reflection trace delay and the ordinary trace delay. This lower trace should finish in such situation on the critical frequency as in the case of the left panel of the Figure 9. But in the right panel of Figure 9 it does not finish at the critical frequency but continues to the end of the frequency band of the sounder. The possible explanation of such reflection trace is given in (Danilkin, 2000) but in general, it is the subject of further discussion and investigation.

CONCLUSION

Some latest results of the topside ionosphere studies were presented. The increase of the topside profile database gives hope for the creation of parameterized empirical model of the topside distribution of vertical ionization. A possible approach and some first results on the way were demonstrated in the paper. The combination of the Epstein function parameterized model of the topside ionosphere with the modern empirical models of the bottom side ionosphere give good possibility for reconstruction of the whole vertical structure of the Earth's ionosphere. Some useful parameters of the topside ionosphere could be derived from such reconstruction, for example, the scale height changes during geomagnetic storms. Some new, not well studied features of the topside ionosphere were demonstrated such as the F3 layer and plasma bubbles in the equatorial ionosphere. It was demonstrated that the F3 layer is well identified not only in equinox but in solar solstice periods also. More statistical studies are necessary to provide the probability models for F3 layer and plasma bubbles spatial and temporal occurrence.

ACKNOWLEDGMENTS

This work was partly supported by the INTAS grant INTAS 2000-0420.

REFERENCES

Ben'kova N.P., M.G.Deminov, A.T.Karpachev N.A.Kochenova Yu.V. Kushnerevsky, V.V.Migulin, S.A.Pulinets, M.D.Fligel. Longitude features shown by topside sounder data and their importance in ionospheric mapping. *Adv.Space Res.* **10**, N 8, p.(8)57- 91(8)66, 1990

Benson R. F., and H. C. Brinton, Ionospheric Plasma Bubble Encounters or ***F*** Region Bottomside Traversals?, *J. Geophys. Res.*, **88**, 6243-6252, 1983

Brinton, H. C., J. M. Grebowsky, and L. H. Brace, The High-Latitude Winter F-Region at 300 km Thermal Plasma

Observations From AE-C *J. Geophys. Res.*, **83**, 4767-4776, 1978

Danilkin N.P., The Results of the Satellite Radio Sounding of the Ionosphere Below the *F*-layer Maximum, *International Journal of Geomagnetism and Aeronomy*, http://eos.wdcb.ru/gpo/2000/gai00351/gai00351.htm, 2000

Depuev V. H., and S. A. Pulinets, Intercosmos-19 observations of an additional topside ionization layer: The F-3 layer, *Adv. Space Res.*, **27**, No. 6/7. p. 1289-1292, 2001

Dyson P. L., and R. F. Benson, Toside Sounder Observations of Equatorial Bubbles, *Geophys. Res. Lett.*, **5**, 795-798. 1978

Hedin A.E., Biondi M.A., Burnside R.G. et al. Revised Global Model of Thermospheric Winds Using Satellite and Ground-Based Observations, *J. Geophys. Res.*, **96**, 7657-7688, 1991.

Karpachev A.T., S.A.Pulinets, V.V.Zarubanov, Modification of IRI Model by the Satellite Data, G4-p-20, XXIV-th General Assembly of the International Union of Radio Science, Abstracts, Kyoto, Japan, p.295, 1993

Karpachev A. T. and N. A. Gasilov, Separation of the Zonal and Meridional Components of the Neutral Wind from the *hmF*2 Longitudinal Variations, *Geomagnetism and Aeronomy*, (English Translation), **40,** No. 4, p. 481-489, 2000

Leitinger , R., S.Radicella, B.Nava., G.Hochegger and J.Hafner; Nequick-COSTprof-NeUoG-plas, a Family of 3D Electron Density Models. COST251 Madeira Workshop Proceedings, pp 75-89, 1999

Muldrew, D. B., F-layer Ionization Troughs Deduced from Alouette Data, *J. Geophys. Res.*, **70**, 2635-2650, 1965

Nava B., S.M. Radicella, S.A.Pulinets, V.Kh.Depuev, Modelling bottom topside electron density and TEC with profile from topside ionograms, *Adv. Space Res.*, **27**, No. 1, p. 31-34, 2001

Pulinets S.A., Prospects of Topside Sounding, in WITS handbook N2, Chapter 3, SCOSTEP Publishing, Urbana, Illinois, p.99-127, 1989

Pulinets S.A., The wave Processes within the Earth's Ionosphere as a Means for Ionospheric Plasma Diagnosis, Doctor of Physics and Mathematics Thesis. IZMIRAN, Moscow, 300 p., 1990

Pulinets, S.A., Seismic Activity as a Source of the Ionospheric Variability, *Adv. Space Res.*, **22**, No 6, p.903-906, 1998

Pulinets S.A., Intercosmos-19 Topside Sounder Data Rescue, XXVIth General Assembly URSI. University of Toronto, Toronto, Ontario, Canada, August 13-21, Abstracts, HG2.1, p. 772, 1999

Pulinets S. A., and A. D. Legen'ka, Pre-seismic Activity Effects on the Equatorial Anomaly, *Geomagnetism and Aeronomy*., (English Translation), **42,** No. 2, p. 181-189, 2002

Radicella, S. M. and M. L. Zhang, The improved DGR Analytical Model of Electron Density Height Profile and Total Electron Content in the Ionosphere, *Annali di Geofisica*, **38**, No. 1, p. 35-41, 1995

Rothkaehl H., A.Kiraga, Z.Klos, S.A.Pulinets, H.F. Radio Noises as a Diagnostic Tool of Global Morphology of the Ionosphere, Proceedings of 11 International Wroclaw Symposium on Electromagnetic Compatibility, Wroclaw, v.2, p.602-605, 1992